# Molecular Diffusion into Ferritin: Pathways, Temperature Dependence, Incubation Time, and Concentration Effects

Xiaoke Yang,* Paolo Arosio,† and N. Dennis Chasteen*

*Department of Chemistry, University of New Hampshire, Durham, New Hampshire 03824, USA, and †Department of Biological and Technological Research, Institute San Raffaele, Via Olgettina 58, 20232 Milano, Italy

ABSTRACT The detailed kinetics of permeation and effusion of small nitroxide spin probe radicals with the protein shells of horse spleen ferritin (HoSF) and human H-chain ferritin (HuHF) and a 3-fold channel variant D131H+E134H of HuHF were studied by electron paramagnetic resonance spectroscopy and gel permeation chromatography under a variety of experimental conditions. The results confirm that the permeation of molecular species of 7–9-Å diameter into ferritin is a charge selective process and that the threefold channels are the likely pathways for entry into the protein. Studies with holoHoSF show that increased temperature increases the rates of penetration and effusion and also increases the concentration of positively charged spin probe accumulated within the protein in excess of that in the external solution. The interior of HoSF is much more accessible to small molecules at physiological temperature of ~40°C than at room temperature. The large activation energy of 63–67 kJ/mol measured for the effusion/penetration and the small diffusion coefficient, $D \sim 5 \times 10^{-22}$ $m^2/s$ at 20°C, corresponding to a time of ~60 min for traversing the protein shell, is consistent with the kinetics of diffusion being largely controlled by the restrictive porosity of the protein itself. An inverse dependence of the first-order rate constant for effusion out of the protein channel on the incubation time used for radical penetration into the protein is attributed to increased binding of the radical within the funnel-shaped channel.

## INTRODUCTION

Ferritin plays a central role in iron homeostasis of a variety of organisms by serving as a reservoir for metabolic iron (Harrison et al., 1998; Chasteen, 1998; Harrison and Arosio, 1996; Proulx-Curry and Chasteen, 1995; Harrison et al., 1986a; Ford et al., 1984). The protein shell of ferritin is composed of 24 subunits assembled to form a hollow cavity of 4:3:2 symmetry with an inner diameter of 8.0 nm (Harrison, and Arosio, 1996; Waldo and Theil, 1996; Ford et al., 1984). Iron is stored in the central cavity in the form of a hydrous ferric oxide mineral core. There are eight hydrophilic and six hydrophobic channels along the threefold and fourfold axes of the protein shell, respectively, which connect the ferritin cavity with its outside environment, making the protein an open system (Harrison et al., 1986b; Ford et al., 1984). It has been suggested that the threefold hydrophilic channels serve as the pathways for iron and other molecular species to enter and leave the protein interior during iron deposition and mobilization (Treffry et al., 1993; Desideri et al., 1991; Stefanini et al., 1989; Wardeska et al., 1986; Levi et al., 1996). Therefore the kinetics of molecular diffusion into and out of the central cavity is an important area of study.

The in vitro mobilization of iron from ferritin involves reduction of the iron(III) core and chelation of the resultant iron(II) (Crichton et al., 1975; Harrison et al., 1991; Watt et al., 1985; Stefanini et al., 1989; Jones et al., 1978). Whether reductants and chelators readily penetrate the protein shell and on what time scale has been a matter of some controversy (Yang and Nagayama, 1995; Webb et al., 1994; Jacobs et al., 1989; Watt et al., 1988; Stuhrmann et al., 1976; Jones et al., 1978; May and Fish, 1977). We addressed this issue in a previous investigation using a variety of nitroxide spin probe radicals as molecular diffusants, which serve as models for the permeability of the protein shell to modestly sized reductants and chelators. The permeability of ferritin to these molecular species and the diffusion kinetics were measured (Yang and Chasteen, 1996). The key advantage of using nitroxides is that the interaction between the nitroxide radical and the superparamagnetic iron core of ferritin eliminates the room-temperature electron paramagnetic resonance (EPR) signal of the radical, providing a means of establishing whether the radical is inside the protein cavity or not. The EPR spectrum can also distinguish between protein-bound and free forms of the radicals according to their microenvironment and mobility (Berliner, 1976; Kocherginsky and Swartz, 1995).

Our previous study with horse spleen ferritin (HoSF) demonstrated that molecular charge and polarity of the diffusants play a critical role in their permeation into ferritin (Yang and Chasteen, 1996). A negatively charged nitroxide was completely excluded from the interior of the protein, whereas positively charged and polar nitroxide radicals penetrated the protein shell to interact with the iron core. An apolar neutral nitroxide radical was found to bind to the exterior of the protein. First-order half-lives for permeation were estimated to be 21–26 min at room temperature. In addition, diffusion was found not to be purely passive. It was observed that the protein tended to accumulate the

*Received for publication 31 August 1998 and in final form 30 December 1999.*

Address reprint requests to N. Dennis Chasteen, Department of Chemistry, University of New Hampshire, Parsons Hall, Durham, NH 03824. Tel.: 603-862-2520; Fax: 603-862-4278; E-mail: ndc@christa.enh.edu.



0006-3495/00/04/2049/11 $2.00

positively charged nitroxide at concentrations in excess of that outside the protein shell when the protein was incubated with the nitroxide for long periods of time (>120 min at 15°C). Longer incubation times lead to slower rates of effusion of the nitroxide out of the protein and caused an unexplained deviation from first-order kinetics.

The present study addresses these previously unexplained phenomena and carries the analysis of the data to a higher level of sophistication, providing new insight into the details of the mechanism of molecular transport across the protein shell. Here, we focus on the temperature dependence of the diffusion and effusion processes and on the influences of incubation time and spin probe concentration on the observed kinetics of effusion. In this work, the partition of the diffusant between the bulk solution phase and the protein is found to increase with increasing incubation temperature, indicating that ferritin becomes more permeable and retains more diffusant at higher temperatures. The measured activation energies for both permeation and effusion are similar and about five times larger than that of the viscosity of water, suggesting that passage of the diffusant across the protein shell is largely controlled by the restrictive porosity of the protein itself. The deviation of the effusion process from simple first-order kinetics when samples are incubated with the diffusant at either high temperatures or long incubation times is adequately described by a two-step three-compartment effusion model. An unexpected dependence on incubation time of the effusion rate constant $k_{-1}$ for movement of the radical down the protein channels is attributed to a variation in binding affinity of the radical for the protein within the channels. A relationship between the first-order rate constant for transport across the protein shell and the diffusion coefficient $D$ is given, allowing an estimate of the latter to be obtained from the kinetic data.

HoSF, recombinant human H-chain ferritin (HuHF), and a variant (D131H+E134H) of HuHF, where the negatively charged glutamate and aspartate residues lining the three-fold channels are replaced by histidines, were used in the present study. Three nitroxide radicals were chosen as diffusants according to their charge and polarity. Among them, one is positively charged, one is polar, and one is negatively charged at neutral pH (Scheme I). The dimensions of these five- and six-membered ring radicals are 7–9 Å (Yang and Chasteen, 1996).

Structures of the Nitroxides at Neutral pH

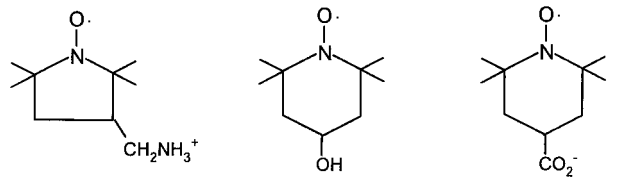


(I) 3-(aminomethyl)-proxyl (II) 4-hydroxy-TEMPO (III) 4-carboxy-TEMPO

SCHEME I

## MATERIAL AND METHODS

### Material

Cadmium-free HoSF was purchased from Boehringer Mannheim (Penzberg, Germany), and Sigma Chemical (St. Louis, MO, USA). HuHF and the variant (D131H+E134H) ferritin was prepared as described previously (Levi et al., 1988; Levi et al., 1987; Treffry et al., 1989). The nitroxide radical 4-hydroxy-TEMPO (TEMPO, 2,2,6,6-tetramethylpiperidine-*N*-oxyl) was purchased from Eastman Kodak Co. (Rochester, NY), 4-carboxy-TEMPO from Aldrich Chemical Co. (Milwaukee, WI) and 3-(aminomethyl)-proxyl (3-aminomethyl-2,2,5,5-tetramethyl-1-pyrrolidinyloxy) from Sigma Chemical Co. MOPS buffer (3-(*N*-morpholino)propanesulfonic acid) buffer was purchased from Research Organics (Cleveland, OH).

### Kinetics measurements

Concentrated nitroxide solutions of 20, 80, and 140 mM for 4-carboxy-TEMPO, 4-OH-TEMPO and 3-(aminomethyl)-proxyl, respectively, were added to the holoferritin solution to form final radical concentrations of 3.0 mM and a protein concentration of approximately 0.1 mM/24mer. The samples were then incubated for specified periods of time from 20 min to 4 h at specific temperatures between 10 and 40°C in a constant temperature bath. After incubation, samples were loaded onto a 1 × 15 cm Sephadex G-25 column equilibrated with 0.05 M MOPS buffer, 0.1 M NaCl, pH 7.0, and quickly separated with an elution time of ~3–4 min. To limit effusion of the radical out of the protein during the separation, the chromatography was carried out at 4°C with the column output directed into a quartz capillary tube running through a quartz dewar in the EPR cavity. The capillary tube was controlled at a specified temperature in the range 10–40°C. EPR measurements of the eluted protein fraction were started immediately after the column separation. The growth of the EPR signal as the nitroxide effused out of the protein was measured as a function of time. Protein concentrations before and after the separation were measured by the Bio-Rad assay (Sedmack and Grossberg, 1977; Bradford, 1976).

A home-assembled X-band EPR spectrometer previously described (Yang and Chasteen, 1996) was used to carry out the EPR measurements at a variety of temperatures. The temperature control consisted of a constant temperature bath with a copper heat-exchange coil, a gas flow meter, and a thermocouple in the EPR quartz dewar containing the capillary. Radical concentrations obtained from EPR measurements at different temperatures were corrected for the effect of temperature ($1/T$ factor) and peak-to-peak line width ($1/\Delta B_{pp}^2$ factor) on the EPR amplitude.

### Models for molecular effusion

The observed effusion kinetics depends on both the incubation and effusion temperatures, and on the incubation time. At low incubation temperature (≤20°C) and short incubation times (≤60 min), the permeation and effusion processes can be represented by a one-step, two-compartment model,

$$A \underset{k_{-1}}{\overset{k_1}{\rightleftharpoons}} A^*, \tag{1}$$

where $A$ and $A^*$ represent the radical in the bulk solution and inside the protein channels, respectively, and $k_1$ and $k_{-1}$ are the corresponding permeation and effusion rate constants for the channels.

In the effusion experiment, the radical concentration outside the protein shell is negligible following chromatographic separation of the protein;

thus, the rate of diffusion back into the protein can be ignored. The effusion process then follows simple first-order kinetics, i.e.,

$$[A] = [A]_e\{1 - \exp(-k_{-1}t)\}, \quad (2)$$

where $[A]$ and $[A]_e$, respectively, represent the measured radical concentration outside the protein at the effusion time $t$ and the radical concentration outside the protein when effusion is complete. Eq. 2 predicts linear log plots for the effusion kinetics of samples prepared with short incubation times ($\lesssim$60 min) as observed (see Figs. 2–4).

In contrast, nonlinear effusion kinetics is seen for samples prepared with long incubation times ($\gtrsim$90 min) or higher incubation temperatures (>20°C) ( see Fig. 6). Under these conditions, a two-step, three-compartment effusion model is required to fit the data:

$$A \underset{k_{-1}}{\overset{k_1}{\rightleftharpoons}} A^* \underset{k_{-2}}{\overset{k_2}{\rightleftharpoons}} A^{**}. \quad (3)$$

Here, $A^{**}$ represents radical inside the protein cavity and $k_2$ and $k_{-2}$ are the first-order rate constants for exchange of the radical between the channels and the cavity. The integrated rate law is given by

$$[A] = [A]_e\left\{\frac{k_{-2}X_2}{k_{-1} - k_{-2}} - (1 - X_2)\right\}\exp(-k_{-1}t) - [A]_e\left\{\frac{k_{-1}X_2}{k_{-1} - k_{-2}}\right\}\exp(-k_{-2}t) + [A]_e, \quad (4)$$

where $X_1$ and $X_2$ ( $= 1 - X_1$) are the mole fractions of radical in the channels ($A^*$) and the cavity ($A^{**}$), respectively. Eq. 4 describes very well the observed deviation in the effusion kinetics from simple first-order at long incubation times or high incubation temperatures, conditions where the mole fraction $X_2$ of radical reaching the cavity becomes significant (see Fig. 6, *inset*).

Eqs. 2 and 4 provide a convenient means of describing the observed diffusion kinetics. However, to relate the apparent rate constants $k_1$ and $k_{-1}$ obtained for diffusion down the protein channels to more fundamental quantities and to demonstrate that diffusion in the protein shell is a first-order process to a good approximation, we use traditional diffusion theory. The kinetics of diffusion out of a slab of thickness $h$ after previously being incubated with the diffusant for a time $t_I$ is derived in the Appendix (Eqs. A7–A9). The first-order rate constant for effusion is related to the diffusion coefficient, $D$, by the expression,

$$k_{-1} = \pi^2 D/h^2, \quad (5)$$

where $h$ corresponds to the thickness of the protein shell. Eq. A9 of the Appendix is derived from a passive diffusion model and predicts linear log plots for effusion times $t > 1/k_{-1}$ as observed (see Figs. 2–4 and A1). Nonlinearity in the log curve at the beginning of effusion (see Fig. A1) from the higher order terms in Eq. A8 are unimportant for the present work because they occur on a time scale comparable to the time required for chromatographic separation of the protein. Thus, any early nonlinear effects are not expected to be seen in the kinetics data obtained, as is the case (see Figs. 2–4).

The activation energy for penetration into the channels can be determined from the amount of diffusant accumulated in the protein for a fixed incubation time at various temperatures. The total amount of diffusant $M$ passing the total cross-sectional area $C$ of the protein channels at $x = 0$ during an incubation time $t_I$ ($\lesssim$60 min) is given by (Crank, 1975)

$$M = C[A]_0(Dt_I/\pi)^{1/2}. \quad (6)$$

Assuming the diffusion constant of the nitroxide is given by the Stokes–Einstein relation for translational diffusion, $D = k_BT/(6\pi\eta r)$ (Jost, 1952), the above equation becomes

$$M = C[A]_0\{k_BTt_I/(6\pi^2\eta r)\}^{1/2}, \quad (7)$$

where $k_B$ is the Boltzmann constant, $T$ is the absolute temperature, $\eta$ is the microviscosity, and $r$ is the molecular radius of the diffusant. Because $\eta$ is proportional to $\exp(E_a/RT)$ (Eyring, 1936), Eq. 7 then becomes

$$M \propto T^{1/2}\exp(-E_a/2RT), \quad (8)$$

where $E_a$ is the activation energy for fluidity. In this treatment, all the resistance to molecular transport experienced by the diffusant is considered to be from the microviscosity $\eta$ of the channels, which is different from the bulk viscosity of water. Eq. 8 indicates that the total amount of diffusant accumulated inside the protein at a given time $t_I$ (the incubation time) is very dependent on temperature and provides a means of measuring the activation energy for diffusional penetration into the protein (see Fig. 5).

## RESULTS

### The diffusion pathway into ferritin

Permeability measurements on both HuHF and HoSF at 40°C showed that the positively charged and the polar radicals penetrate the protein shell, whereas the negatively

**TABLE 1 Final concentrations and average number of different nitroxides in different proteins under similar incubation conditions***

| Protein | 3 (aminomethyl)-proxyl, mM; Number of Radical/protein | 4-carboxy-TEMPO, mM; Number of Radical/protein | 4-OH-TEMPO, mM; Number of Radical/protein |
|---|---|---|---|
| HoSF† | 10.7 ± 0.5 | Not detected | 9.0 ± 0.3 |
| | 0.70 | — | 0.59 |
| HuHF† | 2.5 ± 0.1 | Not detected | 1.7 ± 0.1 |
| | 0.33 | — | 0.22 |
| D131H+E134H‡ | 0.60 ± 0.04 | 0.45 ± 0.03 | 5.2 ± 0.4 |
| | 0.08 | 0.06 | 0.68 |

*Concentrations calculated from EPR measurement and a protein cavity volume of $1.1 \times 10^{-22}$ L for the half-full cavity of HoSF and $2.2 \times 10^{-22}$ L for HuHF and D131H+E134H (Yang and Chasteen, 1996). Iron content of proteins: 2200, 170, and 20 Fe/protein for HoSF, HuHE, and D131H+E134H, respectively. A bulk radical concentration of 3 mM was used during incubation of all samples.

†Incubated with the positively charged 3-(aminomethyl)-proxyl and polar 4-OH-TEMPO radicals for 60 min at 40°C and with the negatively charged 4-carboxy-TEMPO radical for 120 min at 50°C.

‡All radicals incubated for 60 min at 35°C.

charged radical cannot (Table 1), a conclusion consistent with previous work on HoSF at 20°C (Yang and Chasteen, 1996). HoSF accumulates somewhat greater amounts of positively charged 3-(aminomethyl)-proxyl radical and neutral 4-OH-TEMPO radical than does HuHF under the same conditions, probably a consequence of its greater core size, 2200 versus 170 Fe for HuHF and the greater inner surface negative charge of the L-subunit-rich HoSF (Harrison and Arosio, 1996). The average number of nitroxides per protein molecule ranges from 0.0 to 0.70 for the various nitroxides and proteins (Table 1).

When the glutamate and aspartate residues in the threefold channels of HuHF are mutated in the variant E131H+D134H, all three radicals are found to diffuse into the protein (Table 1). In the variant, the neutral radical attains a concentration inside the protein approximately ten times that of both the positively and negatively charged radicals during the 60-min incubation time period. Under the high temperature conditions (40°C) in Table 1, all the radicals accumulate in all of the proteins in significant amounts with the exception of 4-carboxy-TEMPO with either HoSF or HuHF. In some cases, the nitroxide concentration inside the protein exceeds the external 3-mM concentration used in the incubation, indicating that some association with the protein or mineral core occurs. In subsequent work, we focused our studies on the penetration and effusion kinetics of the positively charged 3-(aminomethyl)-proxyl radical with HoSF; this radical shows a greater propensity than the others to accumulate in both HoSF and HuHF.

## Activation energy for effusion

The effusion kinetics was measured at five different effusion temperatures from 20 to 40°C for samples prepared by incubating HoSF with the positively charged radical for 90 min at 20°C. Data for three temperatures are plotted in Fig. 1. Growth in the EPR spectrum corresponding to the 20°C data is presented in the inset. The same maximum concentration of radical was reached for all five samples as measured from the EPR amplitude (Materials and Methods). Under the conditions of these experiments, the effusion obeys first-order kinetics as described by Eq. 2. The corresponding first-order plots for all five temperatures are shown in Fig. 2 with the Arrhenius plot given in the inset. The rate constants and the activation energy for effusion (63.2 kJ/mol) are compiled in Table 2. Calculated activation enthalpy and entropy parameters $\Delta H^{\ddagger} = 60.7$ kJ/mol and $\Delta S^{\ddagger} = -66.8$ J/K-mol are also given.

## Effects of incubation time and radical concentration on effusion

To obtain information on how the incubation time affects the kinetics of effusion, HoSF samples were incubated with

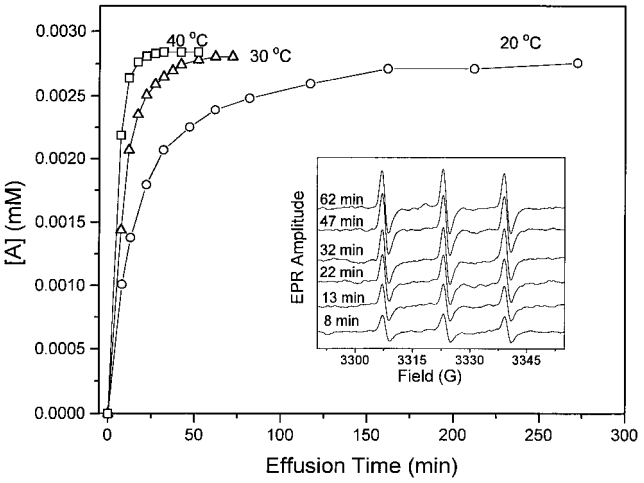


FIGURE 1 Time dependence of the concentration of 3-(aminomethyl)-proxyl effusing from HoSF at the temperatures indicated. Inset: Time evolution of the EPR spectrum for the effusion at 20°C. Conditions for incubation: 0.10 mM holoferritin; 3.0 mM nitroxide; 50 mM MOPS, 0.1 M NaCl, pH 7.0 at 20°C for 90 min. Spectrometer settings: microwave power, 20 mW; frequency, 9.542 GHz; modulation amplitude, 1 G; time constant, 1 s; lock-in amplifier gain, 3 mV.

the positively charged radical at 20°C for varying lengths of time (20–90 min) and the kinetics measured at the same temperature. The results in Fig. 3 reveal that the samples prepared with longer incubation times produce slower first-order effusion rates. A plot of the apparent rate constant $k_{-1}$ as a function of incubation time is given in the inset. Because the protein shell of ferritin is not a homogeneous medium, we explored the possibility that the incubation time dependence of the kinetics might be related to a variation in diffusion coefficient across the protein shell. Simulations for various incubation times were carried out by

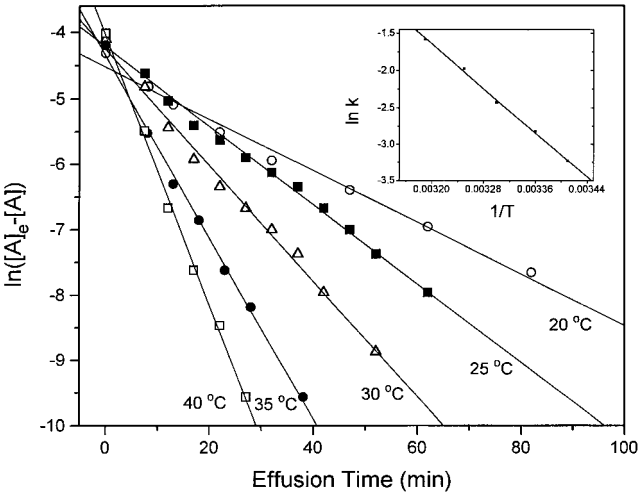


FIGURE 2 First-order plots of the effusion of 3-(aminomethyl)-proxyl from HoSF at the temperatures indicated. Data from Fig. 1. *Inset*: Arrhenius plot.

**TABLE 2 Rate constant for effusion of 3-(aminomethyl)-proxyl along the channels of horse spleen ferritin at different temperatures***

| Temperature (°C) | $k_{-1} \times 10^3$ ($min^{-1}$) |
|---|---|
| 20 | 39.4 ± 1.7 |
| 25 | 59.6 ± 1.3 |
| 30 | 88.4 ± 2.6 |
| 35 | 138.8 ± 3.6 |
| 40 | 205.1 ± 5.3 |
| $E_a$ = 63.2 ± 1.7 kJ/mol, | |
| $\Delta H^{\ddagger}$ = 60.7 kJ/mol, | |
| $\Delta S^{\ddagger}$ = −66.8 J/K-mol | |

*Conditions: nitroxide concentration 3.0 mM; protein concentration 0.1 mM; fixed incubation time 90 min; temperature 20°C.

numerically solving Fick's second law of diffusion (Press et al., 1986), assuming that the diffusion coefficient is a function of position $x$ within the channels or of the concentration of diffusant in the channels. A tenfold variation in $D$ across the protein shell was assumed, but the calculated effusion kinetics were found to be independent of incubation time. Thus, traditional diffusion theory cannot readily explain the variation in $k_{-1}$ with incubation time. The observed reduction in $k_{-1}$ with increasing incubation time likely arises from the fact that diffusion into ferritin is not an entirely passive process as pointed out previously (Yang and Chasteen, 1996), i.e., there is increased binding affinity of the positively charged diffusant for the protein as it moves down the channel, leading to higher activation energy for effusion (see Discussion).

When a twofold difference in radical concentration was used for incubation of the protein at 20°C for 20 min, the first-order rate constant for effusion was found to be unchanged (Fig. 4), a result also consistent with the kinetics model (Materials and Methods). Similarly, the final measured concentration of radical having effused out of the protein is proportional to the incubation concentration as predicted (Fig. 4, *inset*).

## Temperature dependence of degree of association and partitioning of the radical within HoSF

To study the temperature dependence of the degree of partitioning of the radical between the protein and the bulk solution, samples were prepared with the same long incubation time of 3 h at temperatures of 10, 20, 30, and 40°C. Effusion of various samples was conducted initially at 10°C for a period of time, and then the temperature was elevated to 40°C (Fig. 5). When effusion was conducted at 10°C, all the samples ceased releasing further radical after ~175 min. However, upon increasing the effusion temperature to 40°C, additional radical was seen to effuse from the protein with the exception of the sample prepared at an incubation temperature of 10°C (Fig. 5). Thus, for all samples incubated at temperatures higher than 10°C, a higher effusion temperature was required for all of the radical to escape from the protein.

The total amount of radical, $M$, accumulated inside the protein versus the incubation temperature was fitted to Eq. 8 (Fig. 5, *inset*), from which an activation energy $E_a$ = 66.9 ± 2.9 kJ/mol for radical penetration into the protein was obtained. This value is comparable to the value of 63.2 ± 1.7 kJ/mol measured for effusion out of the protein (Table 2).

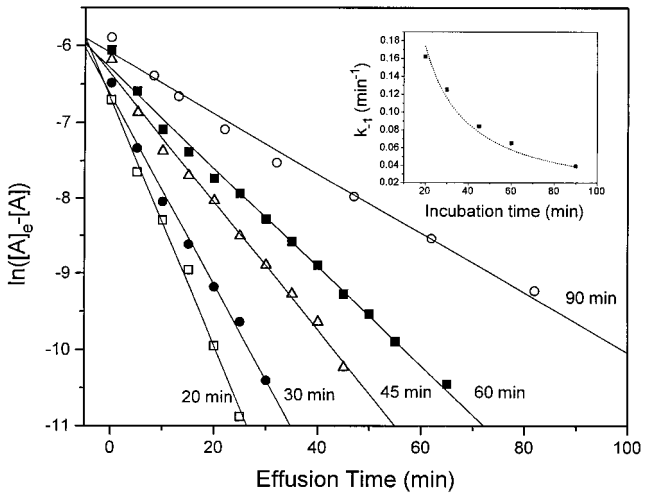


FIGURE 3 First-order plots of the effusion for 3-(aminomethyl)-proxyl from samples prepared at 20°C with the incubation times indicated. *Inset*: Dependence of first-order effusion rate constant on incubation time. Other conditions were the same as for Fig. 1.

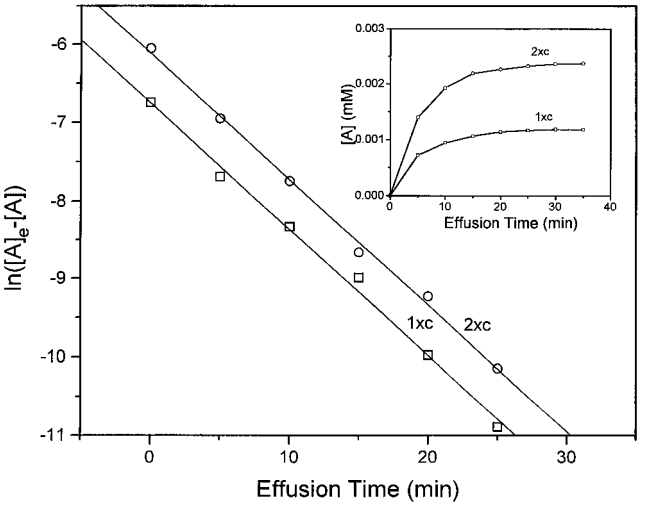


FIGURE 4 First-order plots of the effusion of 3-(aminomethyl)-proxyl from samples incubated with twofold different radical concentrations (3 mM and 6 mM). Conditions, 20 min incubation at 20°C and effusion at 20°C, were the same as for Fig. 1. *Inset*: Time dependence of the radical concentration effusing from samples prepared at the two radical concentrations.

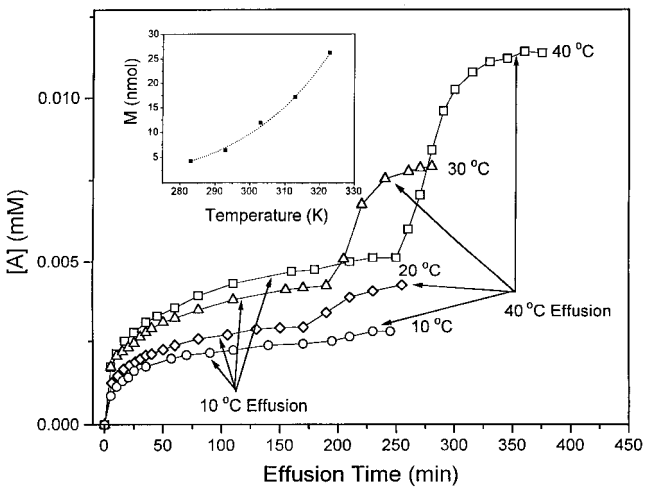


FIGURE 5 Time dependence of the concentration for 3-(aminomethyl)-proxyl effusing from samples incubated for 3 h at the temperatures indicated. The effusion was carried out at 10°C first for about 3 h and then increased to 40°C. *Inset*: Temperature dependence of the amount of radical accumulated in HoSF. The dotted line is fitted according to Eq. 8. Other conditions were the same as for Fig. 1.

## Kinetics of effusion for samples prepared with long incubation times

To characterize the effusion kinetics of samples prepared with long incubation times, HoloHoSF was incubated with the positively charged radical for 4 h at 20, 30, and 40°C. The effusion kinetics was then measured at the same temperature as the incubation. The raw kinetic data are plotted in Fig. 6. The first-order plot for the 40°C data is given in the inset and shows marked deviation from first-order kinetics. The dotted lines in Fig. 6 are the fitted curves according to Eq. 4 for the two-step three-compartment effusion model; the solid line in the inset represents the calculated data using the parameters obtained from the fitting. The model fits the data well. The regression values of $k_{-1}$, $k_{-2}$, $X_1$, and $X_2$ are listed in Table 3 for the three temperatures.

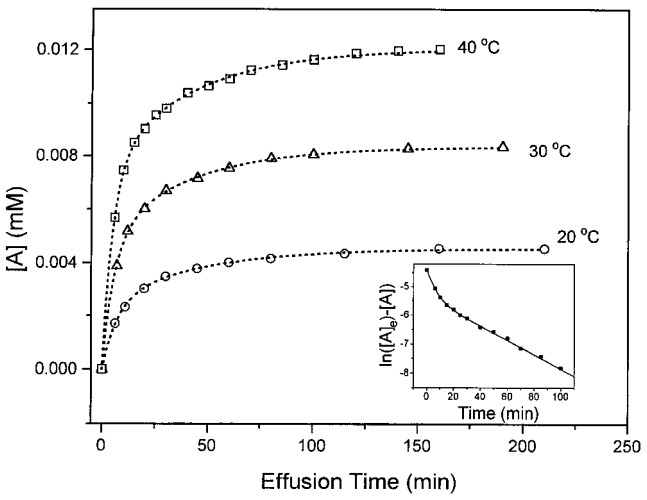


FIGURE 6 Time dependence of the concentration for 3-(aminomethyl)-proxyl effusing from samples prepared with long incubation time (4 h) at the temperatures indicated. The dotted lines are fitted according to Eq. 4. *Inset*: First-order plot of the effusion at 40°C. The solid line is a plot of the calculated data using parameters from the corresponding fitting (Table 3).

## Nitroxide radical accumulation within the cavity of holoferritin as a function of time

To determine the amount of radical reaching the protein cavity as a function of the incubation time, a series of samples were incubated at 20°C for times ranging from 20 to 240 min followed by the immediate measurement of the effusion kinetics at the same temperature. Values of $X_2$ were obtained from curve fitting of the rate data to Eq. 4, from which the corresponding values of the concentration of the radical inside the protein [$A$**] were calculated. A cavity volume of $1.1 \times 10^{-22}$ L for the half-full holoferritin was assumed (Yang and Chasteen, 1996). Figure 7 shows the dependence of [$A$**] on the incubation time. There is an ~60-min lag time before the radical begins to appear in the cavity, whereupon its concentration grows with time, approaching the $[A]_0 = 3$ mM concentration of the external incubation medium.

The lag time is a measure of the time required to traverse the protein shell. The mean square distance $\bar{x}^2$ of diffusion in a time $t_I$ is given approximately by the relationship $\bar{x}^2 = 2Dt_I$ (Jost, 1952). By taking $t_I = 60$ min and assuming $\bar{x}^2 = (22 \times 10^{-10}\ \text{m})^2$, 22 Å being the length of the channel, we estimate an apparent value for $D$ ($\approx 6.7 \times 10^{-22}$ m$^2$/s). Alternatively, we calculate $D = 5.3 \times 10^{-22}$ m$^2$/s from Eq. 5 using the value of $k_{-1} = 0.064$ min$^{-1}$ for the 60-min incubation time, a result in substantial agreement with the value estimated from the lag time. (We note that the length of the funnel-shaped 3–4-Å-diameter channels is usually quoted as 12 Å (Ford et al., 1984). However, for a larger diameter spin probe molecule, the length of the channels extends across the full 22-Å thickness of the protein shell.)

**TABLE 3 Effusion rate constants and mole fractions of 3-(aminomethyl)-proxyl from ferritin based on a two-step model at different temperatures***

| Temperature (°C) | $k_{-2} \times 10^3$ (min$^{-1}$) | $k_{-1} \times 10^3$ (min$^{-1}$) | $X_1$ | $X_2$ |
|---|---|---|---|---|
| 20 | 22.5 ± 1.6 | 136 ± 11 | 0.466 ± 0.034 | 0.534 ± 0.039 |
| 30 | 24.4 ± 1.1 | 168 ± 8.2 | 0.418 ± 0.019 | 0.582 ± 0.026 |
| 40 | 24.7 ± 0.84 | 193 ± 6.8 | 0.379 ± 0.012 | 0.621 ± 0.020 |

*Samples incubated at the temperatures indicated for 4 hr before measuring the effusion kinetics at the same temperature. Concentrations: radical, 3.0 mM; protein, 0.1 mM.

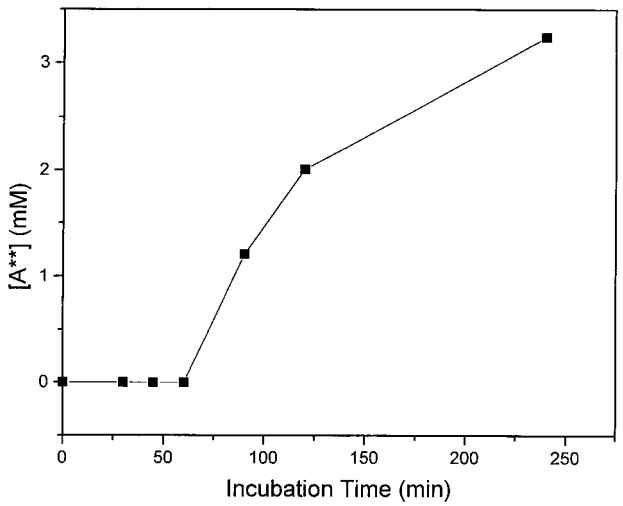


FIGURE 7 Dependence of radical concentration within the cavity of holoferritin on the incubation time. Incubation and effusion were conducted at 20°C.

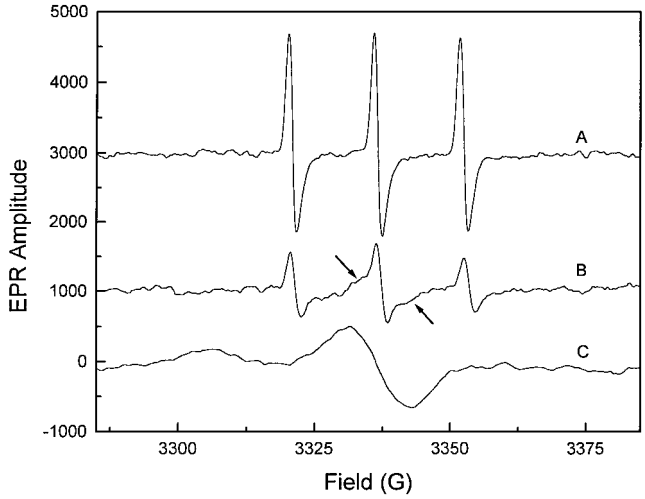


FIGURE 8 EPR spectra of nitroxide with apoHoSF. (*A*) Room temperature spectrum 3 h after separation. (*B*) Room temperature spectrum 7 min after separation. (*C*) Sample frozen right after separation. Arrows denote underlying broad spectral component from an immobilized spin probe. Conditions for incubation: time, 60 min; temperature, 40°C; 0.12 mM apoferritin; 3.0 mM nitroxide; 50 mM MOPS, 0.1 M NaCl, pH 7.0. Spectrometer settings: For room temperature spectrum, microwave power, 20 mW; frequency, 9.542 GHz; modulation amplitude, 1 G; time constant, 1 s; receiver gain, 1 mV; For frozen sample, microwave power, 1 mW; frequency, 9.38 GHz; modulation amplitude, 1.5 G; time constant, 1 s; gain, 1 mV.

### EPR spectroscopy and kinetics of effusion from apoferritin

Figure 8 shows the EPR spectra of apoHoSF after incubation for 1 hr at 40°C with the positively charged radical followed by separation by size exclusion chromatography. The room temperature, *spectrum B*, obtained 7 min after separation, shows two components, a relatively sharp three-line pattern of unequal amplitudes and linewidth characteristic of a spin probe with hindered rotational diffusion and an underlying broad component indicative of a highly immobilized spin probe, cf. the frozen solution, *spectrum C* (Berliner, 1976; Kocherginsky and Swartz, 1995). We attribute the rotationally hindered and immobilized spectral components, respectively, to spin probes weakly bound to the interior of the protein cavity (mole fraction $X_2$) and to those entrained within the channels (mole fraction $X_1$).

Upon standing, the room-temperature (20°C) spectrum in Fig. 8 evolves by a two-phase first-order process ($k_{-1} = 0.103 \pm 0.017$ min$^{-1}$, $k_{-2} = 0.012 \pm 0.001$ min$^{-1}$, $X_1 = 0.498 \pm 0.0045$, $X_2 = 0.502 \pm 0.0046$) into *spectrum A*, which is characteristic of the spin probe in buffer alone. Incubation at the higher temperature of 50°C for 1 hr results in an increase in $X_2$ from 0.502 to 0.604, indicating that a higher fraction of protein-associated probe has reached the cavity.

Unlike the holoprotein, where the magnetism of the core eliminates signals of those spin probe molecules associated with the protein, double integrals of the spectra of the apoprotein in Fig. 8 indicate that the EPR spectrum accounts for all of the spin probe molecules present in the protein. The value of the double integral corresponds to 0.30 nitroxide/apoprotein, which compares with 0.70 nitroxide/holoprotein when the core is present (Table 1) under the same incubation conditions.

It should be noted that the rate constants obtained for the apoprotein differ somewhat from those for holoferritin under similar conditions. In the course of this work, we have noticed some variability in the permeability of apoferritin samples but not in the permeability of holoferritin from different commercial sources. These differences may be due to different methods of preparing the apoprotein from holoferritin by the various manufacturers. Accordingly, the present work has largely focused on studies of the holoprotein.

## DISCUSSION

The experiments reported here have revealed several new properties of molecular diffusion into ferritin. The permeation of small molecules into ferritin at physiological temperature has been confirmed to be a charge-selective process in both H-chain HuHF and mixed H/L-chain HoSF ($H_4L_{20}$), proteins having identical channel structures. The complete exclusion of the negatively charged 4-carboxy-TEMPO radical from the interior of these proteins but its penetration into the cavity of the channel variant D131H+E134H (Table 1) provides strong evidence that the negatively charged threefold channels are the principal pathways for molecular diffusion into ferritin. This conclusion is consistent with our previous work (Yang and Chasteen, 1996) showing that $Tb^{3+}$, which is known to bind in these channels (Harrison et al., 1986a; Treffry and Harrison,

1984), inhibits radical diffusion into ferritin. A number of studies (see Introduction) likewise support the hypothesis that these channels are the primary avenues of entry into the protein cavity. The immobilized component of the spectrum of the apoprotein (Fig. 8) and its slow disappearance as the spin probe escapes from the protein into the bulk solution are consistent with a gradual migration of the probe down the channel. The observation that the channel variant is most permeable to the neutral radical and about equally permeable to both the positive and negative radicals (Table 1) suggests that the imidazole groups of the histidine residues in the threefold channels of the variant are not protonated at the pH 7 of our experiments.

The lesser accumulation of the positive and negative radicals inside the variant compared with the neutral radical (Table 1) is probably a consequence of their slightly larger sizes (Yang and Chasteen, 1996) and of increased steric crowding in the channels from the imidazole groups of histidine in D131H+E134H. In contrast, large differences are not seen between the degrees of penetration of the positive and neutral radicals into the wild type HuHF protein with normal channels (Table 1).

Two populations of radical, i.e., channel and cavity species, are seen in the kinetics of effusion for holoprotein samples incubated for 4 hr at various temperatures (Fig. 6 and Table 3). Simple first-order kinetics is no longer obeyed, and a two-step, three-compartment diffusion model is required to fit the data (Eq. 4 and Fig. 6, *inset*). The mole fraction, $X_2$, of the more slowly effusing population increases with increasing incubation temperature (Table 3) in accord with the trend seen in Fig. 5. A similar phenomenon is seen with the apoprotein (Results), corresponding to a buildup of radical inside the protein cavity.

The data in Fig. 7 are particularly revealing of the process involved in diffusional penetration into the protein. The lag time before the appearance of the radical within the cavity can be attributed to the slow diffusion of the nitroxide down the channel. The movement of the radical within the channels before reaching the cavity is characterized by the rate constants $k_1$ and $k_{-1}$, which are incubation-time dependent, presumably because of increased association of the radical with the protein at longer incubation times (see below).

The apparent value of $D \approx 5 \times 10^{-22}$ m$^2$/s at 20°C for ferritin, which is an average $D$ across the protein shell, indicates that access of the radical to the interior of the protein is very restricted. $D$ for ferritin is many orders of magnitude smaller than the value of $D = k_B T/(6\pi\eta r) \sim 3 \times 10^{-9}$ m$^2$/s predicted from the Stokes–Einstein equation for the translational diffusion of a radical of 7–9-Å diameter in water. This large difference cannot be accounted for by the small fraction ($\sim 2 \times 10^{-4}$) of the external surface area of the protein shell occupied by the sum of the cross-sectional areas of the 8 threefold channels. Furthermore, the estimated value of $D$ for ferritin is comparable to the value of $D = 2.1 \times 10^{-21}$ m$^2$/s measured for the penetration of the nitroxide TEMPO-choline into dimyristoylphosphatidylcholine vesicles (Marsh et al. 1976). Thus, we conclude that ferritin is rather impermeable to the modestly sized diffusants used in this work. This finding is in accord with the small diameter of 3–4 Å of the threefold channels relative to the 7–9-Å size of the diffusant.

The measured activation energy, ~63–67 kJ/mol, for effusion/penetration in ferritin (Figs. 2 and 5; Table 2) is substantially larger than the activation energy of 12.1 kJ/mol for the fluidity of water (Ewell and Eyring, 1937). The large activation energy and small diffusion coefficient for the protein implies that the radical experiences considerable frictional drag as it traverses the protein shell. The activation energy probably represents the energy associated with a fluctional increase in the pore size of the channel or release of the radical from binding sites within the channel, allowing the diffusant to gradually traverse the protein shell. The relatively large negative entropy of activation, $\Delta S^{\ddagger} = -66.8$ J/K-mol, is consistent with the formation of an associated species in the transition state, namely entrapment of the spin probe within the channel. Recent kinetic and crystallographic studies of the L134P variant of amphibian H-chain ferritin have led to the proposal that the threefold channel functions as a dynamic aperture (Takagi et al., 1998), an idea in accord with the data presented here.

Another important finding is that the effusion kinetics carries information about the incubation conditions used in sample preparation and depends on both the incubation temperature and incubation time. That effusion is truly a first-order process with a rate constant, $k_{-1}$, independent of radical concentration is demonstrated by the data in Figs. 3 and 4 and the equations derived in the Appendix. However, also of interest, is the observation that $k_{-1}$ is inversely proportional to the incubation time, $t_I$, (Fig. 3, *inset*), which we attribute to increased binding in the channels. The funnel shape of the channels and their negative charge are consistent with this idea, as is the fact that $k_1 > k_{-1}$ (Yang and Chasteen, 1996). In this connection, recent calculations predict an electrostatic potential gradient from the outside of the threefold channel leading to the interior of the protein (Douglas and Ripoll, 1998). Such a gradient would predict an increased binding affinity of the positively charged radical with increased incubation time and hence a decrease in $k_{-1}$. An increase in activation energy of only 3 kJ/mol when the incubation time changes from 20 to 90 min, or only 5% of the measured value of 63 kJ/mol, can account for the observed variation in effusion rate constant with incubation time seen in Fig. 3. Although traditional diffusion theory cannot explain the variation in activation energy with incubation time, it does predict rather well the kinetic behavior of diffusion for a given incubation time and yields a reasonably consistent value of the diffusion coefficient, $5.3 \times 10^{-22}$ versus $6.7 \times 10^{--2}$ m$^2$/s (see Results).

The results from the high-temperature incubation, low-temperature effusion experiments indicate that entrapment

of the radical by the protein itself or its iron core is very temperature dependent. The data in Fig. 5 show that the radicals in the protein have two final environments when incubation is carried out at temperatures above 10°C. There is a weakly associated population of radicals that diffuses out of the protein at 10°C and a more tightly associated population requiring a higher temperature for effusion. The total amount of radical accumulated in the protein when the incubation is carried out at 40°C is about 3 times that when the incubation is done at 10°C (Fig. 5). We postulate that the more strongly associated population of positively charged radical is associated with the core as is known to occur with other cations (Price and Joshi, 1983; Fleming and Joshi, 1987). HoSF with a mineral core of 2200 iron atoms attains a radical concentration of 10.7 mM in its interior (Table 1), compared with 1.9 mM concentration for the apoprotein under the same incubation conditions. Because the tightly associated population of radicals is formed only in the holoprotein and when the incubation is carried out at an elevated temperature (>10°C) and requires an elevated temperature (40°C) to effuse out of the protein, entrapment of the radical within the core itself probably has occurred (Fig. 5). Some weak association of the spin probe with the protein also occurs as evidenced by the rotationally hindered component of the EPR spectrum of the apoprotein (Fig. 8, *spectrum B*).

One important issue in ferritin research is whether reducing agents must come in direct contact with the mineral core to bring about reduction of the iron. The concentration of iron within a protein shell of 80 Å inner diameter containing 2200 iron atoms is about 14 M. Thus, if reduction were to require direct contact of the reductant with the core, a reductant with a half-life of ~60 min for traversing the protein shell would take over a year at a bulk solution concentration of 1 mM to completely reduce the core. The larger reduced flavin mononucleotide, $FMNH_2$, (10.6 × 13.3 × 14.8 Å versus 7.0 × 7.1 × 8.4 Å for 3-(aminomethyl)proxyl [Yang and Chasteen, 1996]), is a reasonably efficient reductant for ferritin iron, which has been suggested to penetrate the protein shell during reduction (Jones et al., 1978). In actuality, it probably reduces the iron by long-range electron transfer as suggested by the work of Watt and coworkers (1988).

The time of ~60 min for penetration reported here is longer than our previous estimate of 21–26 min (Yang and Chasteen, 1996). The latter values are an underestimate because the calculated half-lives were based on the values of $k_1$ and $k_{-1}$ obtained for short incubation times. Regardless of the precise value of the time required to traverse the protein shell, which depends on the charge and size of the diffusant, we conclude that molecular penetration to the interior of the protein is a slow process.

Finally, we note that the measured rate constant $k_{-1}$ in Table 3 shows little temperature dependence because each experiment was performed at the same temperature for both incubation and effusion (20, 30, or 40°C). To measure energies of activation for penetration or effusion, the temperature of either incubation or effusion has to be fixed while the other is varied (Figs. 2 and 5).

In summary, the present work has revealed several aspects of the diffusion kinetics of ferritin previously unknown. The effect of channel mutations on changing the charge-selective permeability of the protein, the relatively low permeability of the protein to small molecules, the large activation energies for penetration and effusion, the inverse dependence of the effusion rate constant for traveling along the channels on incubation time, the presence of populations of channel and cavity species entrained within the protein, and the role of the core in radical uptake have been demonstrated for the first time. The results of the present work highlight the complexities involved in carrying out proper studies of molecular diffusion into ferritin and emphasize the importance of the protein shell, the restrictive nature of the threefold channels and the binding properties of the channels and mineral core in governing the kinetic properties of the protein.

## APPENDIX

### Diffusional penetration through a slab

We treat the diffusion of the nitroxide down the channel to the central cavity of ferritin as a special case of one-dimensional diffusion. For diffusional penetration through a slab of thickness $h$ (the thickness of the protein shell), the concentration distribution $C(x, t)$ across the slab at any given time $t$ is given by

$$C(x,t) = C_1 + (C_2 - C_1)\cdot\frac{x}{h} + \frac{2}{\pi}\sum_{n=1}^{\infty}\frac{C_2\cos n\pi - C_1}{n}\cdot\sin\frac{n\pi x}{h}\cdot\exp(-n^2kt) + \frac{2}{h}\sum_{n=1}^{\infty}\sin\frac{n\pi x}{h}\cdot\exp(-n^2kt)\cdot\int_0^h f(x')\sin\frac{n\pi x'}{h}\,dx'. \quad \text{(A1)}$$

The expression for $C(x, t)$ is obtained from solution of Fick's second law, $\partial(C(x,t)/\partial t = D\partial^2(C(x,t)/\partial x^2$, under the boundary conditions $C = C_1$ at $x = 0$ and $C = C_2$ at $x = h$ for all $t$, and $C = f(x')$ for $0 < x' < h$ at $t = 0$ (Daynes, 1920). $k$ is the rate constant for diffusion, i.e., $k = \pi^2 D/h^2$ where $D$ is the diffusion coefficient. $x = 0$ and $x = h$ correspond to the outer and inner surfaces of the protein shell, respectively, and $C_1$ and $C_2$ are the concentrations at these surfaces. $f(x')$ is the concentration distribution within the slab before commencing the diffusion experiment. Because, initially, there is no diffusant within the protein shell, $f(x')$ is zero. We assume that $C_2 = 0$ because there is no diffusant within the protein cavity initially, and, once it reaches the cavity, its concentration is low due to binding to the inner surface of the protein shell and to the mineral core.

After exposure of the protein to the diffusant at a concentration $C_1$ for an incubation time $t_l$, Eq. A1 becomes

$$C(x, t_l) = C_1 - C_1 \frac{x}{h} - \frac{2C_1}{\pi} \sum_{n=1}^{\infty} \frac{1}{n} \sin \frac{n\pi x}{h} \cdot \exp(-n^2 k t_l). \quad \text{(A2)}$$

Eq. A2 gives the concentration distribution within the protein shell at the incubation time $t_l$ just before commencing the effusion experiment.

## Effusion out of the slab

For effusion out of the slab, the concentration in the bulk solution is zero, i.e., $C_1 = 0$ in Eq. A1, and the initial concentration within the slab is $f(x')$ and is given by $C(x', t_l)$ from Eq. A2, where we have replaced $C_1$ with $C_1'$ to distinguish it from the new $C_1$ for the bulk solution. Substituting Eq. A2 for $f(x')$ in Eq. A1 with only the last term being retained, the others being zero, gives

$$C(x, t) = \frac{2}{h} C_1' \sum_{n=1}^{\infty} \sin \frac{n\pi x}{h} \cdot \exp(-n^2 k t) \cdot \int_0^h \left[ \sin \frac{n\pi x'}{h} - \frac{x'}{h} \sin \frac{n\pi x'}{h} - \frac{2}{\pi} \sum_{n=1}^{\infty} \frac{1}{n} \sin^2 \frac{n\pi x'}{h} \cdot \exp(-n^2 k t_l) \right] dx'. \quad \text{(A3)}$$

Integration of Eq. A3 yields

$$C(x, t) = \frac{2C_1'}{\pi} \sum_{n=1}^{\infty} \frac{1}{n} \sin \frac{n\pi x}{h} \cdot \exp(-n^2 k t)[1 - \exp(-n^2 k t_l)]. \quad \text{(A4)}$$

The flux $F$ out of the protein shell into the bulk solution in mole/m$^2$-s, is given by Fick's first law, $F = D(\partial C(x, t)/\partial x)_{t,\ x=0}$. Differentiation of Eq. A4 gives an expression for the flux,

$$F = \frac{2C_1' D}{h} \sum_{n=1}^{\infty} [1 - \exp(-n^2 k t_l] \cdot \exp(-n^2 k t). \quad \text{(A5)}$$

The total amount of diffusant $M_t$ escaping per m$^2$ cross-sectional area during the time $t$ is given by

$$M_t = \int_0^t F \, dt = \frac{2C_1' h}{\pi^2} \sum_{n=1}^{\infty} \frac{1}{n^2} [1 - \exp(-n^2 k t_l)] \cdot [1 - \exp(-n^2 k t)]. \quad \text{(A6)}$$

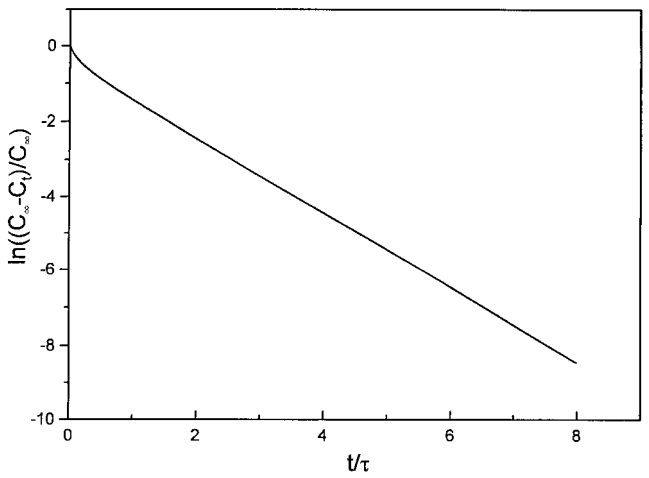


FIGURE A1 Plot of $\ln[(C_\infty - C_t)/C_\infty]$ versus $t/\tau$ ($\tau = 1/k = h^2/\pi^2 D$) for the parameters: $C_1' = 3$ mol/m$^3$, $t_l = 3600$ s, $h = 22 \times 10^{-10}$ m, and $D = 5.3 \times 10^{-22}$ m$^2$/s in Eqs. A7 and A8.

For kinetic analysis, we use the two expressions,

$$M_\infty = \frac{2C_1' h}{\pi^2} \sum_{n=1}^{\infty} \frac{1}{n^2} [1 - \exp(-n^2 k t_l)], \quad \text{(A7)}$$

$$M_\infty - M_t = \frac{2C_1' h}{\pi^2} \sum_{n=1}^{\infty} \frac{1}{n^2} [1 - \exp(-n^2 k t_l)] \cdot \exp(-n^2 k t). \quad \text{(A8)}$$

Eq. A8 is a sum of exponentials that depend on the effusion time $t$ with coefficients that depend on the incubation time $t_l$. For effusion times $t > 1/k$, the $n = 1$ term dominates, leading to first-order kinetics, namely,

$$\ln[(M_\infty - M_t)/M_\infty] \approx kt. \quad \text{(A9)}$$

Figure A1 illustrates a plot of $\ln[(C_\infty - C_t)/C_\infty]$ ($= \ln[(M_\infty - M_t)/M_\infty]$) versus $t/\tau$ where $C_t$ is the concentration of diffusant in the bulk medium at the time $t$, and $\tau = 1/k$ is the diffusional relaxation time. The early nonlinear part of the graph is due to the higher-order terms in the sum of exponentials. The linear portion of the graph enables the diffusional rate constant $k = \pi^2 D/h^2$ to be determined (Eq. A9). Note that the slope, and therefore the rate constant, is independent of the incubation time. Therefore, the first-order plot carries no information about the incubation time of the sample except in the early nonlinear portion of the graph.

This work was supported by grant: R37 GM20194 of the National Institute of General Medical Sciences (N.D.C.) and the CNR Target Project on Biotechnology (P.A.).

## REFERENCES

Berliner, L. J. 1976. Spin Labels, Theory and Applications. Academic Press, New York.

Bradford, M. M. 1976. A rapid and sensitive method for the quantitation of microgram quantities of protein utilizing the principle of protein–dye binding. *Anal. Biochem.* 72:248–254.

Chasteen, N. D. 1998. Ferritin. Uptake, storage and release of iron. *In* Metal Ions in Biological Systems. Iron Transport and Storage in Micro-

organisms, Plants, and Animals. Vol. 35. A. Sigel and H. Sigel, editors. Marcel Dekker, Inc., New York. 479–514.

Crank, J. 1975. The Mathematics of Diffusion. 2nd Ed. Clarendon Press. Oxford. 20–21, 32, 37–38.

Crichton, R. R., M. Wauters, and F. Roman. 1975. Ferritin iron uptake and release. *In* Proteins of Iron Storage and Transport in Biochemistry and Medicine. R. R. Crichton, editor. North Holland/Elsevier, Amsterdam. 287–294.

Daynes, H. A. 1920. The process of diffusion through a rubber membrane. *Proc. Roy. Soc. A.* 97:286–307.

Desideri, A., S. Stefanini, F. Polizio, R. Petruzzelli, and E. Chiancone. 1991. Iron entry route in horse spleen apoferritin: involvement of the three-fold channels as probed by selective reaction of cysteine-126 with the spin label 4-maleimido-tempo. *FEBS Lett.* 287:10–14.

Douglas, T., and D. R. Ripoll. 1998. Calculated electrostatic gradients in recombinant human H-chain ferritin. *Protein Sci.* 7:1083–1091.

Ewell, R. H., and H. Eyring. 1937. Theory of the viscosity of liquids as a function of temperature and pressure. *J. Chem. Phys.* 5:726–736.

Eyring, H. 1936. Viscosity, plasticity, and diffusion as examples of absolute reaction rate. *J. Chem. Phys.* 4:283–291.

Fleming, J., and J. G. Joshi. 1987. Ferritin: isolation of aluminum-ferritin complex from brain. *Proc. Natl. Acad. Sci. USA.* 84:7866–7870.

Ford, G. C., P. M. Harrison, D. W. Rice, J. M. A. Smith, A. Treffry, J. L. White, and J. Yariv. 1984. Ferritin: design and formation of an iron-storage molecule. *Phil. Trans. Roy. Soc. (Lond.).* 304:551–565.

Harrison, P. M., G. C. Ford, D. W. Rice, J. M. A. Smith, A. Treffry, and J. L. White. 1986a. The three-dimensional structure of apoferritin: a framework controlling ferritin's iron storage and release. *In* Frontiers in Bioinorganic Chemistry. A. V. Xavier, editor. VCH, Weinheim. 268–277.

Harrison, P. M., P. C. Hempstead, P. J. Artymiuk, and S. C. Andrews. 1998. Structure–function relationships in the ferritins. *In* Metal Ions in Biological Systems. Iron Transport and Storage in Microorganisms, Plants, and Animals. Vol. 35, A. Sigel and H. Sigel, editors. Marcel Dekker, Inc., New York, 435–478.

Harrison, P. M., A. Treffry, and T. H. Lilley. 1986b. Ferritin as an iron-storage protein: mechanisms of iron uptake. *J. Inorg. Biochem.* 27:287–293.

Harrison, P. M., S. C. Andrews, P. J. Artymiuk, G. C. Ford, J. R. Guest, J. Hirzmann, D. M. Lawson, J. C. Livingstone, J. M. A. Smith, and A. Treffry. 1991. Probing structure–function relations in ferritin and bacterioferritin. *Adv. Inorg. Chem.* 36:449–486.

Harrison, P. M., and P. Arosio. 1996. Ferritins: molecular properties, iron storage function and cellular regulation. *Biochim. Biophys. Acta Bioenerg.* 1275:161–203.

Jacobs, D. L., G. D. Watt, R. B. Frankel, and G. C. Papaefthymiou. 1989. Redox reactions associated with iron release from mammalian ferritin. *Biochemistry.* 28:1650–1655.

Jones, T., R. Spencer, and C. Walsh. 1978. Mechanism and kinetics of iron release from ferritin by dihydroflavins and dihydroflavin analogues. *Biochemistry.* 17:4011–4017.

Jost, W. 1952. Diffusion in Solids, Liquids, Gases. Academic Press. New York. 25–30, 35–38, 45–46.

Kocherginsky, N., and H. M. Swartz. 1995. Nitroxide Spin Labels, Reactions in Biology and Chemistry. CRC Press, New York.

Levi, S., G. Cesareni, P. Arosio, R. Lorenzetti, M. Soria, M. Sollazo, A. Albertini, and R. Cortese. 1987. Characterization of human ferritin H chain synthesized in *Escherichia coli*. *Gene.* 51:269–274.

Levi, S., A. Luzzago, G. Cesareni, A. Cozzi, F. Franceschinelli, A. Albertini, and P. Arosio. 1988. Mechanism of ferritin iron uptake: activity of the H-chain and deletion mapping of the ferroxidase site. A study of iron uptake and ferroxidase activity of human liver, recombinant H-chain ferritins, and of two H-chain deletion mutants. *J. Biol. Chem.* 263: 18086–18092.

Levi, S., P. Santambrogio, A. Cozzi, and P. Arosio. 1996. Evidence that residues exposed on the three-fold channels have active roles in the mechanism of ferritin iron incorporation. *Biochem. J.* 317:467–473.

Marsh, D., A. Watts, and P. F. Knowles. 1976. Evidence for phase boundary lipid. Permeability of tempo-choline into dimyristoylphosphatidylcholine vesicles at the phase transition. *Biochemistry.* 15: 3570–3578.

May, M. E., and W. W. Fish. 1977. The restrictive nature of apoferritin channels as measured by passive diffusion. *In* Protein of Iron Metabolism. E. B. Brown, P. Aisen, J. Fielding, and R. R. Crichton, editors. Grune and Stratton, New York. 31–38.

Press, W. H., B. P. Flannery, S. A. Teukolsky, and W. T. Vettering. 1986. Numerical Recipes. The Art of Scientific Computing. Cambridge University Press, Cambridge, 635–642.

Price, D. J., and J. G. Joshi. 1983. Ferritin: binding of beryllium and other divalent metal ions. *J. Biol. Chem.* 258:10873–10880.

Proulx-Curry, P. M., and N. D. Chasteen. 1995. Molecular aspects of iron uptake and storage in ferritin. *Coord. Chem. Rev.* 144:347–368.

Sedmack, J. J., and S. E. Grossberg. 1977. A rapid sensitive, and versatile assay for protein using Coomassie Brilliant Blue G250. *Anal. Biochem.* 79:544–552.

Stefanini, S., A. Desideri, P. Vecchini, T. Drakenberg, and E. Chiancone. 1989. Identification of the iron entry channels in apoferritin. Chemical modification and spectroscopic Studies. *Biochemistry.* 28:378–382.

Stuhrmann, H. B., J. Haas, K. Ibel, M. H. J. Koch, and R. R. Crichton. 1976. Low angle neutron scattering of ferritin studied by contrast variation. *J. Mol. Biol.* 100:399–413.

Takagi, H., D. Shi, Y. Ha, N. M. Allewell, and E. C. Theil. 1998. Localized unfolding at the junction of the three ferritin subunits. *J. Biol. Chem.* 273:18685–18688.

Treffry, A., P. M. Harrison, A. Luzzago, and G. Cesareni. 1989. Recombinant H-chain ferritins: effects of changes in the 3-fold channels. *FEBS Lett.* 247:268–272.

Treffry, A., E. R. Bauminger, D. Hechel, N. W. Hodson, I. Nowik, S. J. Yewdall, and P. M. Harrison. 1993. Defining the roles of the threefold channels in iron uptake, iron oxidation and iron-core formation in ferritin: a study aided by site-directed mutagenesis. *Biochem. J.* 296: 721–728.

Treffry, A., and P. M. Harrison. 1984. Spectroscopic studies on the binding of iron, terbium, and zinc by apoferritin. *J. Inorg. Biochem.* 21:9–20.

Waldo, S., and E. C. Theil. 1996. Ferritin and iron biomineralization. *Comp. Supramol. Chem.* 5:65–89.

Wardeska, J. G., B. Viglione, and N. D. Chasteen. 1986. Metal ion complexes of apoferritin: evidence for initial binding in the hydrophilic channels. *J. Biol. Chem.* 261:6677–6683.

Watt, G. D., R. B. Frankel, and G. C. Papaefthymiou. 1985. Reduction of mammalian ferritin. *Proc. Natl. Acad. Sci. USA.* 82:3640–3643.

Watt, G. D., D. Jacobs, and R. B. Frankel. 1988. Redox reactivity of bacterial and mammalian ferritin: is reductant entry into the ferritin interior a necessary step for iron release? *Proc. Natl. Acad. Sci. USA.* 85:7457–7461.

Webb, B., J. Frame, Z. Zhao, M. L. Lee, and G. D. Watt. 1994. Molecular entrapment of small molecules within the interior of horse spleen ferritin. *Arch. Biochem. Biophys.* 309:178–183.

Yang, D., and K. Nagayama. 1995. Permeation of small molecules into the cavity of ferritin as revealed by proton nuclear magnetic resonance relaxation. *Biochem. J.* 307:253–256.

Yang, X., and N. D. Chasteen. 1996. Molecular diffusion into horse spleen ferritin: a nitroxide radical spin probe study. *Biophys. J.* 71:1587–1595.